LA-UR-13-27101 (Accepted Manuscript)

Engineering Interface Structures and Thermal Stabilities via SPD Processing in Bulk Nanostructured Metals

Zheng, Shijian
Carpenter, John S.
McCabe, Rodney J.
Beyerlein, Irene J.
Mara, Nathan A.

Provided by the author(s) and the Los Alamos National Laboratory (2016-09-01).

To be published in: Scientific Reports

DOI to publisher's version: 10.1038/srep04226

Permalink to record: http://permalink.lanl.gov/object/view?what=info:lanl-repo/lareport/LA-UR-13-27101

Disclaimer:
Approved for public release. Los Alamos National Laboratory, an affirmative action/equal opportunity employer, is operated by the Los Alamos National Security, LLC for the National Nuclear Security Administration of the U.S. Department of Energy under contract DE-AC52-06NA25396. Los Alamos National Laboratory strongly supports academic freedom and a researcher's right to publish; as an institution, however, the Laboratory does not endorse the viewpoint of a publication or guarantee its technical correctness.

SCIENTIFIC REPORTS

OPEN

SUBJECT AREAS:
MECHANICAL PROPERTIES
METALS AND ALLOYS
SYNTHESIS AND PROCESSING

Received
27 January 2014

Accepted
10 February 2014

Published
27 February 2014

Correspondence and requests for materials should be addressed to S.J.Z. (sjzheng@lanl.gov; sizhengsj@gmail.com) or J.S.C. (carpenter@lanl.gov)

Engineering Interface Structures and Thermal Stabilities via SPD Processing in Bulk Nanostructured Metals

Shijian Zheng[1], John S. Carpenter[2], Rodney J. McCabe[2], Irene J. Beyerlein[3] & Nathan A. Mara[1]

[1]Center for Integrated Nanotechnologies, MPA-CINT, Los Alamos National Laboratory, Los Alamos, NM 87545, USA, [2]Materials Science and Technology Division, MST-6, Los Alamos National Laboratory, Los Alamos, NM 87545, USA, [3]Theoretical Division, T-3, Los Alamos National Laboratory, Los Alamos, NM 87545, USA.

Nanostructured metals achieve extraordinary strength but suffer from low thermal stability, both a consequence of a high fraction of interfaces. Overcoming this tradeoff relies on making the interfaces themselves thermally stable. Here we show that the atomic structures of bi-metal interfaces in macroscale nanomaterials suitable for engineering structures can be significantly altered via changing the severe plastic deformation (SPD) processing pathway. Two types of interfaces are formed, both exhibiting a regular atomic structure and providing for excellent thermal stability, up to more than half the melting temperature of one of the constituents. Most importantly, the thermal stability of one is found to be significantly better than the other, indicating the exciting potential to control and optimize macroscale robustness via atomic-scale bimetal interface tuning. Taken together, these results demonstrate an innovative way to engineer pristine bimetal interfaces for a new class of simultaneously strong and thermally stable materials.

The materials community has been, and will continue to be, in search of metals that can maintain exceptionally high strength at extremely high temperatures to satisfy harsher application requirements[1,2]. To date, nanostructured metals have exhibited much higher strengths than possible with traditional coarse-grained metals[3–8].

However, achieving extraordinary strength together with high temperature tolerance in bulk ($> cm^3$) nanostructured pure metals has been unattainable with current synthesis methods[9–12]. Metallic multilayers fabricated by bottom–up processes, such as physical vapor deposition (PVD), have high strength and thermal stability, but are thin films with overall micrometer thicknesses. Nanocrystalline metals produced by top-down process, such as SPD, have high strength and are in bulk form, but they are thermally unstable even at slightly above room temperatures[13,14]. These mechanical methods produce nanocrystalline metals that contain a high density of crystallographically disordered, non-equilibrium grain boundaries (interfaces), which with minimal thermal stimulus promote grain coarsening[15–17]. In efforts to engineer stable interfaces, alloying has been shown to stabilize grain boundaries in nanocrystalline metals[2,18–20]. Yet still, the long sought after ability to control the interface properties down to the atomic scale via directed manufacturing has yet to be achieved.

Recently, in synthesizing bulk two-phase nanocomposites via SPD, we discovered that a preferred interface develops uniformly across the bulk that possesses a highly ordered atomic structure with few detectable extrinsic defects[21,22]. The pristine interfaces had two exciting implications. First, it implies microstructural stability in extreme conditions. Prior work on PVD foils[23] has shown that highly ordered bimetal interfaces are much more robust against thermally-induced instabilities than ordinary grain boundaries. Accordingly, by virtue of the pristine interfaces induced in the SPD process, the SPD composites have proven remarkably strong[24], thermally stable[21], and radiation resistant[25]. Second, it implies that this processing technique could in fact be used to tune the atomic structures of interfaces.

Here we demonstrate the ability to control interface character at the atomic scale in bulk metallic materials via SPD. Bulk Cu-Nb nanolayered composites with equal individual layer thicknesses were made by a well-developed SPD method that accumulative roll bonding (ARB) consisting of repeated roll bonding, cutting, stacking and rolling[26].

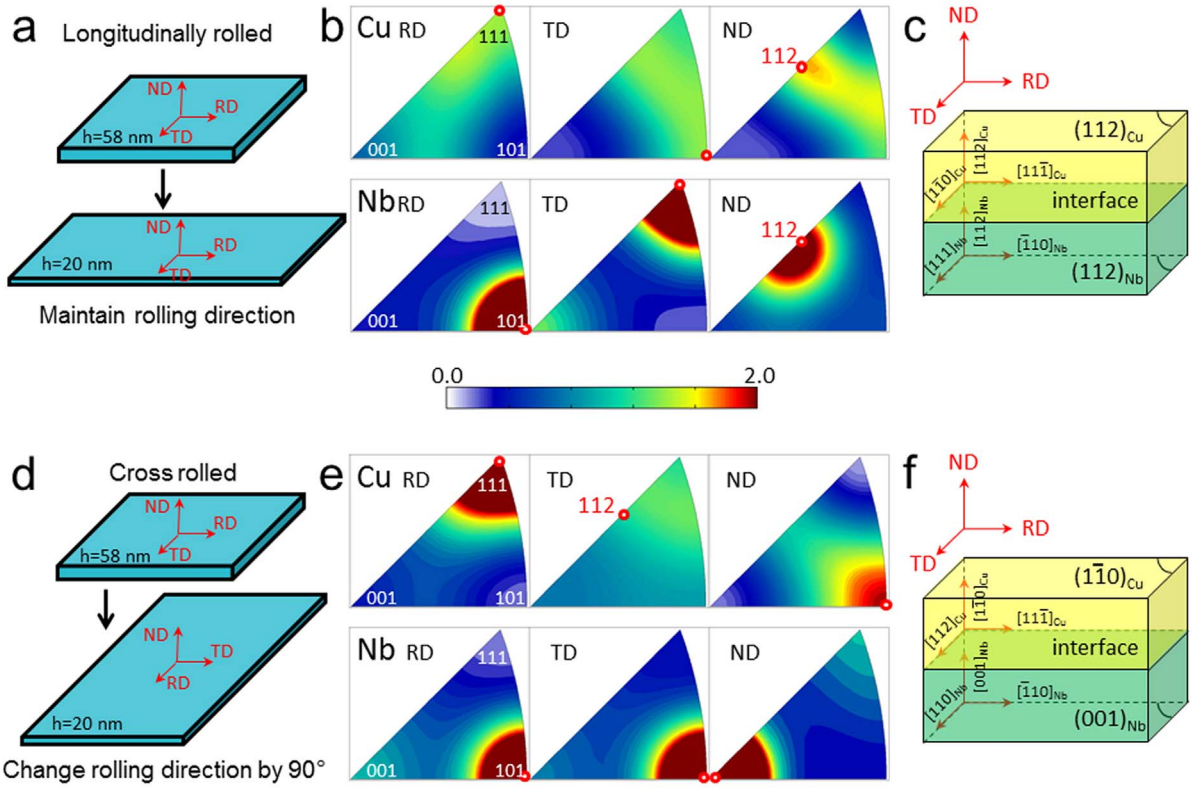

Figure 1 | Two straining pathways generating two materials containing completely different textures and interfaces. Schematic diagrams of the two ARB pathways used: (a) ARB-LR (longitudinally rolled), (d) ARB-CR (cross-rolled); Inverse pole figures of Cu and Nb, in which the main texture components are marked with red dots: (b) 20 nm ARB-LR, (e) 20 nm ARB-CR; the predominant interface structures that (c) (112)[11$\bar{1}$]Cu||(112)[$\bar{1}$10]Nb in 20 nm ARB-LR and (f) (1$\bar{1}$0)[11$\bar{1}$]Cu||(001)[1$\bar{1}$0] in 20 nm ARB-CR resulting from pathways (a) and (d), respectively.

Results

To tune the interface feature, we alter the SPD processing pathway. ARB material was made by maintaining the rolling direction in each step until individual Cu and Nb layer thicknesses (h) were reduced to 58 nm. As demonstrated in figure 1a, to synthesize the ARB-LR (longitudinally rolled) material with 20 nm average individual layer thickness, we continued to roll the h = 58 nm ARB material while preserving the same rolling direction as used from the start of the process. In contrast, the ARB-CR (cross-rolled) material with 20 nm individual layer thickness was produced by rolling the 58 nm ARB material with a new rolling direction rotated 90° in-plane as shown in figure 1d. The two ARB materials experienced the same final total strain of 11.51.

Using neutron diffraction, we found that the two processing pathways generate two completely different textures. The measured textures for the 20 nm composites are presented in the form of inverse pole figures (IPFs) in the rolling direction (RD), transverse direction (TD) and normal direction (ND) of the processed sheet. As an indication of their stability, the same textures are generated at 30 nm ARB-LR and 30 nm ARB-CR textures, respectively (supplementary figure 1). Analysis of these textures reveals that both deviate from conventional single phase Cu and Nb rolling textures[27]. In figure 1b, the 20 nm ARB-LR material contains a predominant {112}<111>Cu||{112}<110>Nb texture (where the crystal planes and directions are written parallel to the {rolling plane}-<rolling direction>), which is consistent with the texture of 58 nm ARB-LR material (Supplementary figure 2). Additionally, the minor texture component {551}<1 1 10> of the Cu phase is due to interface-facilitated Cu twinning, which initiates when the individual layer thickness reduces below 50 nm[21,27–29]. The change in processing pathway induced a completely different texture, as seen in figure 1e. Mean-field crystal plasticity simulations of the cross-rolling successfully predicted these textures, suggesting that this abrupt alteration is accommodated solely by crystallographic slip (see supplement and supplementary figure 3). Remarkably, the Cu and Nb textures of the ARB-CR material are exceptionally sharp (figure 1e), suggesting a preferential interface character of {110}<111>Cu||{001}<110>Nb. The stable and prevailing interfaces suggested by the texture in the ARB-LR and ARB-CR samples are illustrated in figures 1c and 1f.

To study the morphologies of the grains and layers at these fine scales, we used transmission electron microscopy (TEM). For all layers in both the ARB-LR (figure 2a) and ARB-CR (figure 2b) materials, only one crystal spanned the distance between two adjacent interfaces. Another notable feature of both materials is the planarity of the Cu-Nb interfaces and the regularity of layer thicknesses. Thus, changing the processing pathway on the nanomaterial to make the ARB-CR nanomaterial preserved the lamellar architecture without roughening or breaking up the layers. The TEM analysis also revealed that unlike the ARB-CR material, the ARB-LR material contains many deformation twins in the Cu layers (figure 2a), which leads to its distinct texture development, as mentioned above. Twinning occurs in the ARB-LR sample because its interfaces and grain orientations favor it, whereas those in the ARB-CR sample do not[29,30].

To examine the interfacial atomic structures, high resolution (HR) TEM analysis was carried out on many regions throughout these samples. Figure 2c and 2d display typical HRTEM micrographs of the {112}<111>Cu||{112}<110>Nb interface within the 20 nm ARB-LR material and the {110}<111>||{001}<110> interface within the 20 nm ARB-CR material, respectively. These prevailing interfaces are illustrated in figures 1c and 1f. The orientation relationships of these two interfaces are Kurdjumov-Sachs (K-S) and Nishiyama-Wasserman (N-W), respectively. Unlike the familiar K-S and N-W fcc/bcc interfaces that arise from thermodynamic

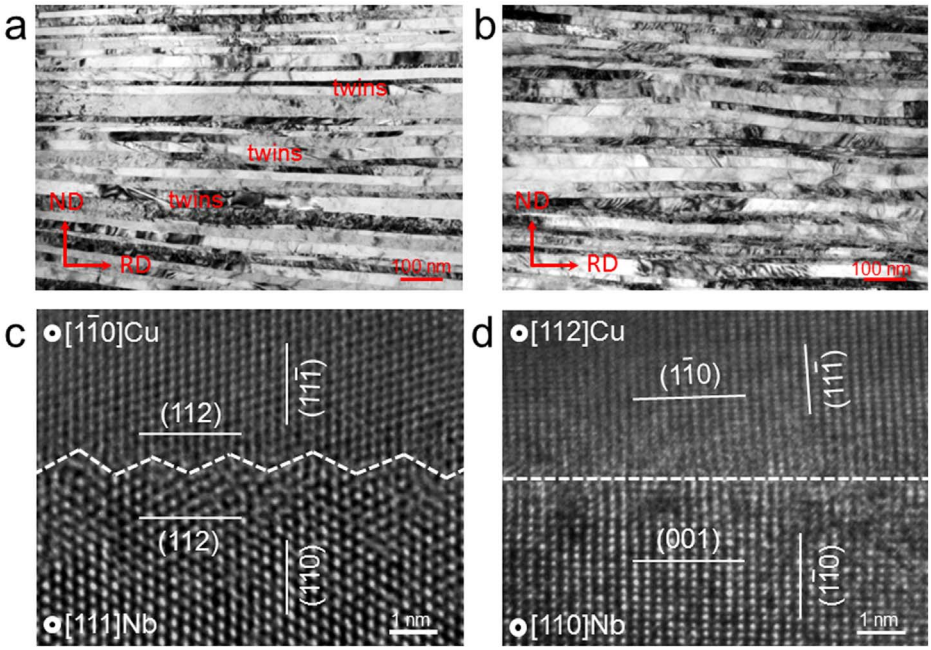

Figure 2 | Typical bright field TEM images showing nanolamellar morphologies of the (a) 20 nm ARB-LR sample and (b) 20 nm ARB-CR sample. A large number of twins are present in the Cu phase of 20 nm ARB-LR material, but not in the 20 nm ARB-CR material. Representative HRTEM images of the predominant interface in the (c) 20 nm ARB-LR material, which is noticeably faceted and (d) 20 nm ARB-CR material, which is atomically flat.

processes[24] whose interface planes correspond to the closest packed planes, the {111}Cu and {110}Nb planes, the mechanically driven interfaces emerging in these samples join the fcc and bcc crystals at different interface planes, namely the {112}Cu||{112}Nb and {110}Cu||{001}Nb planes. Most intriguingly, both interfaces are found by HRTEM to be atomically ordered. While the former {112}Cu||{112}Nb K-S interface is comprised of a regular array of facets, the latter {110}Cu||{001}Nb N-W interface is atomically flat. Recent fundamental studies have shown that this difference profoundly affects the ability of the interface to act as a source for dislocations and deformation twins[29,31,32], the two main carriers of plastic deformation. Thus, by atomically altering interface structure we have a newfound way of controlling the mechanical properties of nanomaterials.

At this point, we have demonstrated for the first time that two distinct atomically ordered interfaces can be created by altering the bulk mechanical processing pathway. To assess the quality of these interfaces, we test their stability in microstructure and hardness with respect to high temperature annealing. Figure 3a shows experimental results from nanoindentation tests before and after high-temperature annealing. Both materials maintain their high hardness, as well as their layered morphologies and layer thickness even after exposure to 500°C for one hour (supplementary figures 4b, 4f, 5c and 5d). This thermal stability far surpasses that of single-phase nanocrystalline Cu fabricated also by SPD techniques[13]. Materials made by non-equilibrium SPD techniques are expected to be thermally unstable because they contain high-energy interfaces[12,17]. Remarkably, our SPD materials have an uncharacteristically high-temperature tolerance that is comparable to that of Cu-Nb nanolayered films fabricated via PVD[23], which are comprised of low-energy, semi-coherent Cu-Nb interfaces. It is also superior to that of nano-twinned Cu, which contain a high density of low-energy, coherent twin boundaries[33]. Thus the two interfaces we have formed via mechanical means possess the same thermal stabilities as interfaces formed via thermal equilibrium processes such as PVD.

Surprisingly, the two materials possess different thermal stabilities at a higher temperature. The ARB-CR maintains its hardness up to 600°C, unlike the ARB-LR 20 nm material which exhibits a 19.3% drop. To explain the difference, the increment in the average layer thickness with annealing temperature is plotted in figure 3b based on TEM measurement (Supplementary figures 4 and 5). Comparing the variation of hardness and average layer thickness reveals a significant dependence of strength on length scale. After annealing at 600°C for one hour, the average layer thickness of the ARB-LR materials doubled while the ARB-CR material only increased by 5%. In repeating the experimental analysis for higher temperatures, we find that the threshold of thermal stability for the ARB-CR material lies between 600°C and 700°C for one hour annealing (supplementary figures 4 h and 5 h).

A key question that arises is why the two ARB materials exhibit different thermal stabilities. To address this question, we first examined the atomic structures of the bimetal interfaces that prevail over these materials--the {112}<111>Cu||{112}<110>Nb and {110}<112>Cu||{001}<110>Nb interfaces–after heating using HRTEM. Remarkably, both interfaces after heating at 600°C were stable. Specifically many important structural properties, including the atomic scale features of facets or flatness, the chemical sharpness, and crystallography, were maintained. Second, in light of earlier reports that intra-layer grain boundaries are relatively unstable[23], we considered possible differences in their grain boundary density. Using a unique, high-resolution "wedge-mounting" electron backscatter diffraction (WM-EBSD)[34], we were able to correlate grain boundary density to the statistical distribution of grain sizes in the two in-plane directions, the TD and the RD. To ensure statistically significant and representative data, we confirmed that the textures from the WM-EBSD technique are consistent with those from neutron diffraction (supplementary figure 6).

Grain size distributions for both Cu and Nb in the original TD and RD reference frame (prior to cross-rolling) are illustrated in figure 4. For the 58 nm ARB-LR material, on average the grains are shaped like "planks" with RD:ND:TD ratios of 33 : 1 : 7 and 83 : 1 : 16 in the Cu and Nb, respectively. The analysis is repeated for the h = 30 nm ARB-LR and ARB-CR samples since the h = 20 nm materials are too fine for the WM-EBSD technique. However, it is reasonable to

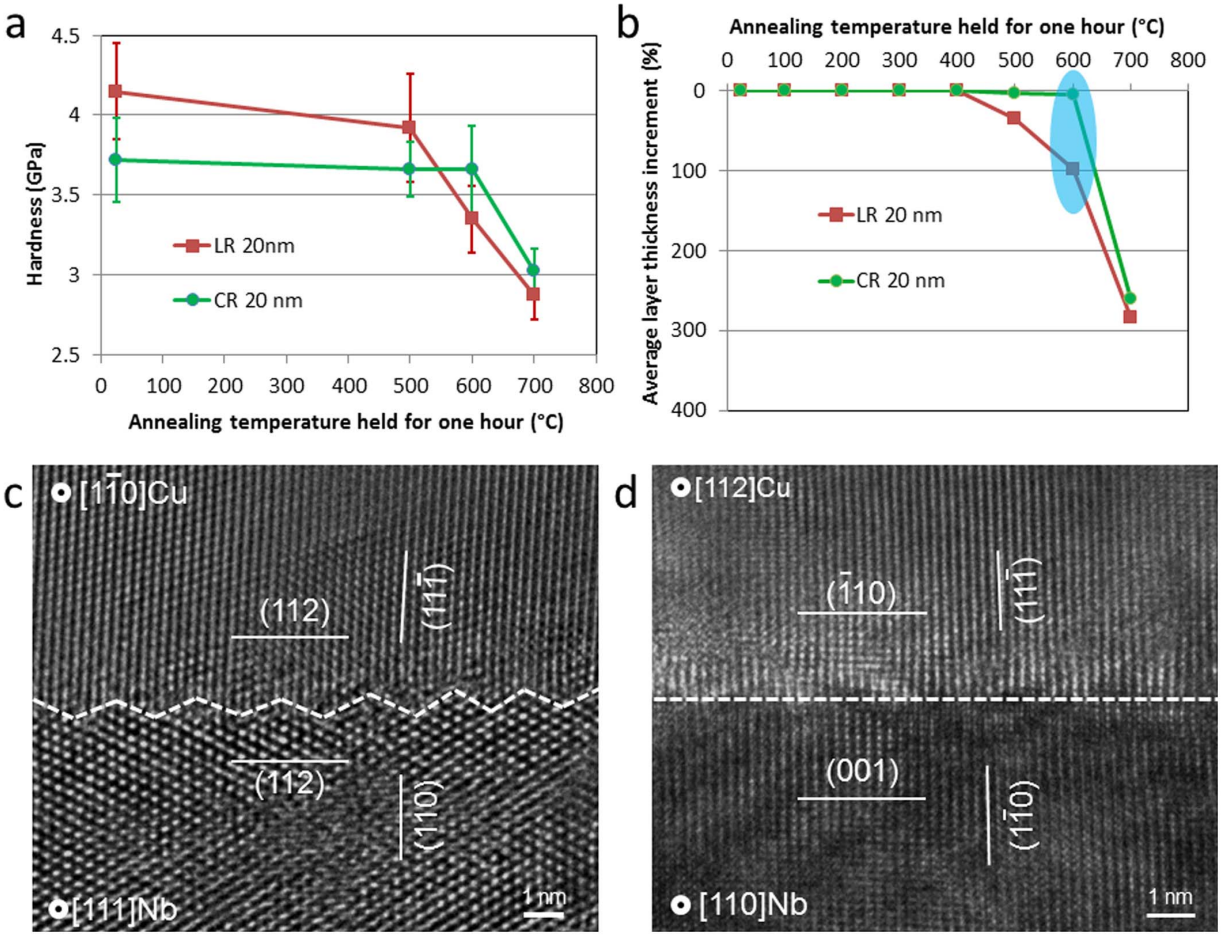

Figure 3 | Outstanding thermal stability of nanomaterial strength and their interface structures. (a) Hardness reduction as a function of annealing temperature; (b) percentage increase in average layer thickness as a function of annealing temperatures; (c) typical HRTEM image of the 20 nm ARB-LR material after annealing at 600°C for one hour showing the same atomic faceted structure as before annealing (figure 2(c)); (c) typical HRTEM image of the 20 nm ARB-CR material after annealing at 600°C for one hour showing the same atomically flat structure as before annealing (figure 2(d)).

deduce that the trends in aspect ratios in the h = 30 nm are consistent with those in the h = 20 nm materials. The results show that the basic grain shapes in the h = 58 nm are maintained in the h = 30 nm ARB-LR material. In contrast, for the 30 nm ARB-CR material, we find 'pancake-shaped' grains, where the average length of the grains in the original RD has not changed, but the average length in the original TD has increased three-fold. Due to the extremely large aspect ratios, we conclude that the grain boundary fraction in both materials is exceedingly small. In the ARB-CR material this fraction is even smaller compared to the ARB-LR material. Evidently, the differences of grain boundary fraction seen in figure 4 lead to important differences in their thermal stabilities seen in figure 3. This suggests that controlled SPD processing is a profitable way to improve thermal stability of materials by simultaneously increasing the stable interface fraction and decreasing unstable grain boundary fraction.

Discussion

In conclusion, we report here the unprecedented ability to control bimetal interface structures at the atomic scale in bulk nanostructured composites via SPD. Specifically, two different SPD synthesis pathways are shown to both produce interfaces with preferred orientation relationships and distinct atomic features. Moreover, both interfaces are stable up to 600°C. Thermal stability of nanostructured metals can be improved by increasing the stable interface region that is grain-boundary-free. These findings open up new ways of engineering interfaces that are stable and lead to exceptional properties.

Methods

Material fabrication. The ARB processing technology can fabricate bulk nanomaterials appropriate for industry scale applications. The ARB process used for this work started with one polycrystalline sheet of reactor grade Nb (99.97% pure, ATI-Wah Chang) of thickness h = 2 mm and two oxide-free high conductivity Cu sheets (99.99% pure, Southern Copper and Supply) of thickness h = 1 mm. All the sheets were 20 cm long and 6.5 cm wide. After a five-minute ultrasonic acetone bath followed by wire brushing to facilitate bonding, the Cu and Nb sheets were stacked in a sandwich-like structure (Cu-Nb-Cu) for the first roll-bonding step. A 2-high rolling mill (Waterbury-Farrel, Brampton, Ontario, Canada) was used in this roll-bonding step with an approximate 60% reduction in thickness. Following each roll-bonding step, a repeating sequence of halving, cleaning, restacking, and roll bonding was performed until the average layer thickness was 200 nm. From 200 nm, the samples were only subjected to conventional rolling with a 10% decrease in total sample thickness per rolling step. After individual Cu and Nb layer thicknesses were reduced to 58 nm, the material was cut into two pieces. One piece was rolled in the same rolling direction as used from the start of the process until the individual layer thickness reduced to 20 nm (ARB-LR). The other piece was rotated 90° in-plane and rolled in the new rolling direction to get the ARB-CR material with individual layer thickness of 20 nm. The whole ARB process was carried out at room temperature.

Texture analysis. Textures of the samples were measured via neutron diffraction on the High Pressure Preferred Orientation (HIPPO)[27] time-of-flight diffractometer at the Los Alamos Neutron Science Center at Los Alamos National Laboratory. Samples with a surface size of 1.5 cm^2 were mounted in a way that the Cu-Nb interfaces were perpendicular to the incoming neutron beam and the rolling direction of the sample was parallel with the notch. Five banks of detector panels set at 2θ = 150°, 120°, 90°, 60°, and 40°, respectively, were used to collect diffraction data, while each bank created a full rotation (with regards to the neutron beam direction) of detection coverage. Each sample was rotated to specific angles of ω = 0°, 67.5°, and 90° to increase the coverage of the pole

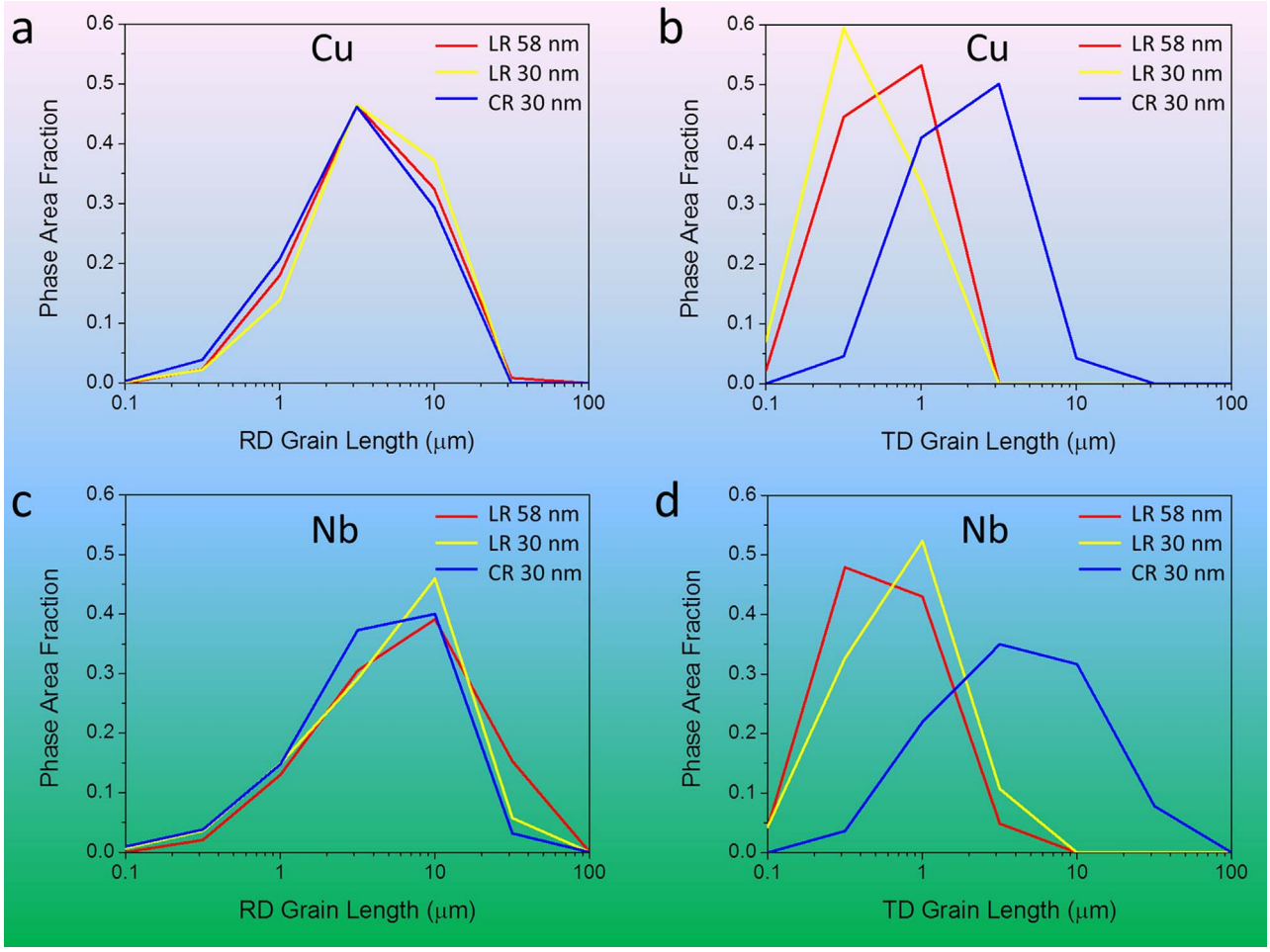

Figure 4 | Grain size distributions measured by the WM-EBSD technique, indicating different grain shapes, as well as grain boundary densities, of the 30 nm ARB-LR and 30 nm ARB-CR materials. Cu phase: (a) RD and (b) TD; Nb phase: (c) RD and (d) TD. For comparison with the ARB-LR materials, the RD and TD directions labeled for the 30 nm ARB-CR material correspond to the original directions before cross-rolling.

figures during the collection. A Rietveld refinement on 150 neutron diffraction patterns was performed on the program MAUD[27]. A 10° resolution of the Rietveld refinement was chosen in order to simultaneously fit all the diffraction patterns to an orientation distribution function (ODF). Then, the rolling, normal, and transverse directions were properly aligned via the Matlab-based mtex program[35]. Additionally, mtex was used for analysis of the ODFs and plotting the inverse pole figures (IPFs).

TEM investigation. All TEM samples were prepared by a conventional cross-sectioning method consisting of mechanical thinning and ion milling on a Gatan precision ion polishing system (PIPS). TEM and STEM were carried out on a Cs-corrected Titan 80–300 (FEI). All the TEM samples were viewed down the TD direction, so that the images comprise RD and ND directions. It is worth noting that the ARB-CR samples were also viewed down the new TD direction after the rotation.

Heating treatment. Annealing was performed at a 500°C, 600°C and 700°C for one hour under vacuum (4E-06 Torr) in a 3310 Series Furnace (Applied Test Systems, Inc., Butler, PA). The samples were cooled under vacuum.

Hardness test. All hardness tests were carried out on a Nanoindenter XP (Agilent). Hardness measurements were made continuously in the continuous stiffness measurement (CSM) mode with a target strain rate of 0.05 1/s. Average hardness values were calculated from 25 separate indents, which included hardness data from 1500 nm to 2000 nm depths, which is the depth range a steady-state hardness value been found. In order to ensure an accurate tip area function for the Berkovich tip, a silica standard sample was used for calibration before and after indentation of each sample. In addition, the onset of loading, which is an indicator of displacement into sample, was verified for each indent.

WM-EBSD. To obtain fine-scale information but over a large area of the material, we made use of wedge-mounting electron backscatter diffraction (WM-EBSD), where crystal orientation and phase data can be uniquely retrieved at fine scales (~30 nm). Using WM-EBSD allows us as many as 6 data points across a 30 nm layer on average, which is much more statistically significant, especially for nanocomposites consist of multi-phases.

1. Lu, K. The Future of Metals. *Science* **328**, 319–320 (2010).
2. Chookajorn, T., Murdoch, H. A. & Schuh, C. A. Design of Stable Nanocrystalline Alloys. *Science* **337**, 951–954 (2012).
3. Valiev, R. Nanostructuring of metals by severe plastic deformation for advanced properties. *Nat. Mater.* **3**, 511–516 (2004).
4. Lu, L., Chen, X., Huang, X. & Lu, K. Revealing the Maximum Strength in Nanotwinned Copper. *Science* **323**, 607–610 (2009).
5. Bringa, E. M. *et al.* Ultrahigh strength in nanocrystalline materials under shock loading. *Science* **309**, 1838–1841 (2005).
6. Wang, Y. M., Chen, M. W., Zhou, F. H. & Ma, E. High tensile ductility in a nanostructured metal. *Nature* **419**, 912–915 (2002).
7. Zhu, Y. T. & Langdon, T. G. The fundamentals of nanostructured materials processed by severe plastic deformation. *JOM* **56**, 58–63 (2004).
8. Meyers, M. A., Mishra, A. & Benson, D. J. Mechanical properties of nanocrystalline materials. *Prog. Mater. Sci.* **51**, 427–556 (2006).
9. Lu, K. Nanocrystalline metals crystallized from amorphous solids: Nanocrystallization, structure, and properties. *Mater. Sci. Eng. R-Rep.* **16**, 161–221 (1996).
10. Valiev, R. Z., Islamgaliev, R. K. & Alexandrov, I. V. Bulk nanostructured materials from severe plastic deformation. *Prog. Mater. Sci.* **45**, 103–189 (2000).
11. Nix, W. D. Mechanical-properties of thin-films. *Metall. Trans. A* **20**, 2217–2245 (1989).
12. Estrin, Y. & Vinogradov, A. Extreme grain refinement by severe plastic deformation: A wealth of challenging science. *Acta Mater.* **61**, 782–817 (2013).
13. Jiang, H. G., Zhu, Y. T., Butt, D. P., Alexandrov, I. V. & Lowe, T. C. Microstructural evolution, microhardness and thermal stability of HPT-processed Cu. *Mater. Sci. Eng. A* **290**, 128–138 (2000).
14. Horita, Z., Fujinami, T., Nemoto, M. & Langdon, T. G. Equal-channel angular pressing of commercial aluminum alloys: Grain refinement, thermal stability and tensile properties. *Metall. Mater. Trans. A* **31**, 691–701 (2000).

15. Dao, M., Lu, L., Asaro, R. J., De Hosson, J. T. M. & Ma, E. Toward a quantitative understanding of mechanical behavior of nanocrystalline metals. *Acta Mater.* **55**, 4041–4065 (2007).
16. Mabuchi, M., Ameyama, K., Iwasaki, H. & Higashi, K. Low temperature superplasticity of AZ91 magnesium alloy with non-equilibrium grain boundaries. *Acta Mater.* **47**, 2047–2057 (1999).
17. Horita, Z., Smith, D. J., Nemoto, M., Valiev, R. Z. & Langdon, T. G. Observations of grain boundary structure in submicrometer-grained Cu and Ni using high-resolution electron microscopy. *J. Mater. Res.* **13**, 446–450 (1998).
18. Bachmaier, A., Kerber, M., Setman, D. & Pippan, R. The formation of supersaturated solid solutions in Fe-Cu alloys deformed by high-pressure torsion. *Acta Mater.* **60**, 860–871 (2012).
19. Edwards, D., Sabirov, I., Sigle, W. & Pippan, R. Microstructure and thermostability of a W-Cu nanocomposite produced via high-pressure torsion. *Philos. Mag.* **92**, 4151–4166 (2012).
20. Bachmaier, A. & Pippan, R. Generation of metallic nanocomposites by severe plastic deformation. *Int. Mater. Rev.* **58**, 41–62 (2013).
21. Zheng, S. J. *et al.* High-strength and thermally stable bulk nanolayered composites due to twin-induced interfaces. *Nat. Commun.* **4**, 1696 (2013).
22. Lee, S. B., LeDonne, J. E., Lim, S. C. V., Beyerlein, I. J. & Rollett, A. D. The heterophase interface character distribution of physical vapor-deposited and accumulative roll-bonded Cu-Nb multilayer composites. *Acta Mater.* **60**, 1747–1761 (2012).
23. Misra, A., Hoagland, R. G. & Kung, H. Thermal stability of self-supported nanolayered Cu/Nb films. *Philos. Mag.* **84**, 1021–1028 (2004).
24. Beyerlein, I. *et al.* Structure–Property–Functionality of Bimetal Interfaces. *JOM* **64**, 1192–1207 (2012).
25. Han, W. *et al.* Design of Radiation Tolerant Materials Via Interface Engineering. *Adv. Mater.* **25**, 6975–6979 (2013).
26. Saito, Y., Utsunomiya, H., Tsuji, N. & Sakai, T. Novel ultra-high straining process for bulk materials - Development of the accumulative roll-bonding (ARB) process. *Acta Mater.* **47**, 579–583 (1999).
27. Carpenter, J. S. *et al.* Bulk texture evolution of Cu–Nb nanolamellar composites during accumulative roll bonding. *Acta Mater.* **60**, 1576–1586 (2012).
28. Zheng, S. J. *et al.* Deformation twinning mechanisms from bi-metal interfaces as revealed by in-situ straining in the TEM. *Acta Mater.* **60**, 5858–5866 (2012).
29. Beyerlein, I. J., Wang, J., Kang, K., Zheng, S. J. & Mara, N. A. Twinnability of bimetal interfaces in nanostructured composites. *Mater. Res. Lett.* **1**, 89–95 (2013).
30. Werner, E. & Prantl, W. Slip transfer across grain and phase boundaries. *Acta Metall. Mater.* **38**, 533–537 (1990).
31. Beyerlein, I. J., Wang, J. & Zhang, R. Mapping dislocation nucleation behavior from bimetal interfaces. *Acta Mater.* **61**, 7488–7499 (2013).
32. Price, C. W. & Hirth, J. P. Mechanism for generation of screw dislcoations from grain-boundary ledges. *Mater. Sci. Eng.* **9**, 15–& (1972).
33. Anderoglu, O., Misra, A., Wang, H. & Zhang, X. Thermal stability of sputtered Cu films with nanoscale growth twins. *J. Appl. Phys.* **103**, 094322 (2008).
34. Carpenter, J. S., McCabe, R. J., Beyerlein, I. J., Wynn, T. A. & Mara, N. A. A wedge-mounting technique for nanoscale electron backscatter diffraction. *J. Appl. Phys.* **113** (2013).
35. Bachmann, F., Hielscher, R. & Schaeben, H. Texture Analysis with MTEX - Free and Open Source Software Toolbox. *Diffu. Defect Data B: Solid state phenomena* **160**, 63–68 (2010).

Acknowledgments

The authors acknowledge support by the Center for Materials at Irradiation and Mechanical Extremes, an Energy Frontier Research Center funded by the U.S. Department of Energy, Office of Science, Office of Basic Energy Sciences under Award Number 2008LANL1026. IJB and RJM would like to acknowledge support through a Los Alamos National Laboratory Directed Research and Development (LDRD) project ER20140348. This work was performed, in part, at the Center for Integrated Nanotechnologies, an Office of Science User Facility operated for the U.S. Department of Energy, Office of Science. This work has also benefited from the use of the Lujan Neutron Scattering Center at LANSCE, funded by the U.S. Department of Energy, Office of Basic Energy Sciences. The authors appreciate collaboration pertaining to the neutron diffraction work with Dr. Sven C. Vogel of Los Alamos National Laboratory.

Author contributions

S.Z. did the TEM and HRTEM characterization and wrote the manuscript. S.Z. and J.S.C. designed the experiments. J.S.C. and N.A.M. fabricated the composites. J.S.C. carried out neutron diffraction, nanohardness test and annealing. R.J.M. and J.S.C. did the WM-EBSD measurement. I.J.B. performed the simulations. All authors discussed the results and commented on the manuscript.

Additional information

Supplementary information accompanies this paper at http://www.nature.com/scientificreports

Competing financial interests: The authors declare no competing financial interests.

How to cite this article: Zheng, S.J., Carpenter, J.S., McCabe, R.J., Beyerlein, I.J. & Mara, N.A. Engineering Interface Structures and Thermal Stabilities via SPD Processing in Bulk Nanostructured Metals. *Sci. Rep.* **4**, 4226; DOI:10.1038/srep04226 (2014).

This work is licensed under a Creative Commons Attribution-NonCommercial-NoDerivs 3.0 Unported license. To view a copy of this license, visit http://creativecommons.org/licenses/by-nc-nd/3.0